
QUANTIZED APPROXIMATELY ORTHOGONAL RECURRENT NEURAL NETWORKS

Armand Foucault^{*1}, Franck Mamalet^{†2}, and François Malgouyres^{‡1}

¹Institut de Mathématiques de Toulouse, UMR5219. Université de Toulouse, CNRS. UPS IMT, F-31062 Toulouse Cedex 9, France

²Institut de Recherche Technologique Saint Exupéry, Toulouse, France

February 7, 2024

ABSTRACT

Orthogonal recurrent neural networks (ORNNs) are an appealing option for learning tasks involving time series with long-term dependencies, thanks to their simplicity and computational stability. However, these networks often require a substantial number of parameters to perform well, which can be prohibitive in power-constrained environments, such as compact devices. One approach to address this issue is neural network quantization. The construction of such networks remains an open problem, acknowledged for its inherent instability.

In this paper, we explore the quantization of the recurrent and input weight matrices in ORNNs, leading to Quantized approximately Orthogonal RNNs (QORNNs). We investigate one post-training quantization (PTQ) strategy and three quantization-aware training (QAT) algorithms that incorporate orthogonal constraints and quantized weights. Empirical results demonstrate the advantages of employing QAT over PTQ. The most efficient model achieves results similar to state-of-the-art full-precision ORNN and LSTM on a variety of standard benchmarks, even with 3-bits quantization.

1 Introduction

Motivation: Machine learning applications frequently encompass the analysis of time series data, ranging from textual information to audio inputs. Within the realm of deep learning, various Recurrent Neural Network (RNN) architectures, including vanilla RNNs [Rumelhart et al., 1986], Long Short-Term Memory networks (LSTM) [Hochreiter and Schmidhuber, 1997], Gated Recurrent Units (GRUs) [Cho et al., 2014b], Unitary RNNs (URNNs) [Arjovsky et al., 2016] and Orthogonal RNNs (ORNNs) [Mhammedi et al., 2017] have demonstrated notable success in addressing a diverse array of tasks associated with time series data. Additionally, when very large datasets are available, the advent of transformer architectures leveraging attention mechanisms has permitted the further improvement of the performances at the cost of larger models and increased numerical complexity [Vaswani et al., 2017].

These models typically necessitate a substantial number of parameters for optimal performance and entail numerous matrix-vector multiplications during inference, involving matrices and vectors of considerable sizes. However, in numerous instances, there is a need for these models to operate on compact devices with constrained power resources, such as embedded systems. Moreover, these devices might face limitations in memory space for storing extensive model weights. Even in the context of non-embedded systems, constraining the power consumption of RNNs allows for the reduction of system costs and contributes to achieving a more favorable carbon footprint. Ultimately, computational speed proves to be critical for a myriad of applications.

An effective approach to address these challenges is neural network quantization [Gholami et al., 2022]. This technique aims to reduce the number of bits required to represent the weights and/or activations of the network. On one hand,

*firstname.lastname@math.univ-toulouse.fr

†firstname.lastname@irt-saintexupery.com

‡firstname.lastname@math.univ-toulouse.fr

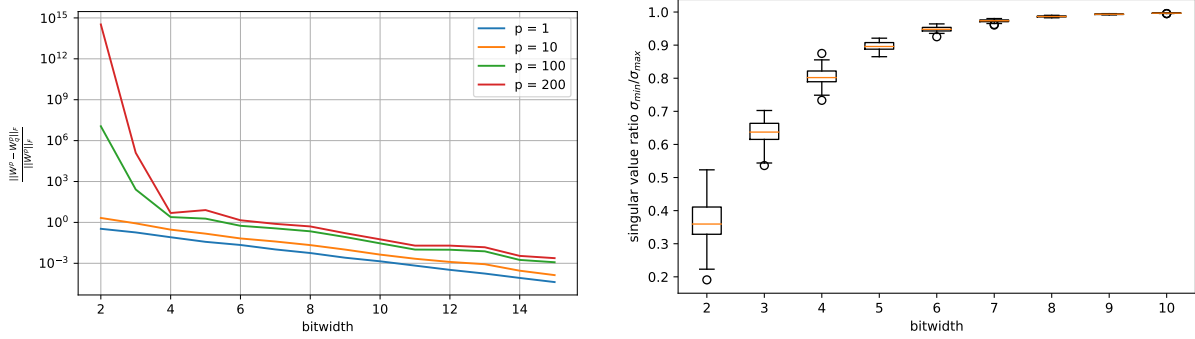


Figure 1: Denote by q_k the quantizer with bitwidth k as defined in Section 3.3, $\sigma_{\min}(q_k(W))$ and $\sigma_{\max}(q_k(W))$ the smallest and largest singular values of the matrix $q_k(W)$ respectively for $W \in \mathbb{R}^{10 \times 10}$ a uniformly sampled orthogonal matrix. (Left) $\frac{\|W^p - q_k(W)^p\|_F}{\|W^p\|_F}$ for various k and powers p . (Right) Boxplots for 1000 random orthogonal matrices W of the ratio $\sigma_{\min}(q_k(W))/\sigma_{\max}(q_k(W))$ for various k .

with appropriate hardware, this accelerates runtime computations, lowers power consumption, and, on the other hand, decreases the amount of space needed for parameter storage. However, depending on the neural network architecture, application, and the chosen quantization strategy, there may be performance degradation [Gupta and Agrawal, 2022, Gholami et al., 2022, Sayed et al., 2023, Yuan and Agaian, 2023].

Our goal is to contribute to the field of quantization of RNNs, with a particular emphasis on addressing long-term dependencies in time series. To do so, we propose and compare four strategies for building Orthogonal or approximately-Orthogonal Neural Networks (ORNNs) with quantized weights. We call them Quantized Orthogonal Recurrent Neural Networks (QORNNs). We assess the methods across various bitwidths on several standard benchmarks.

QORNNs are a tempting solution: Vanilla RNNs are notoriously challenging to train due to issues with vanishing and exploding gradients [Bengio et al., 1994].

LSTM [Hochreiter and Schmidhuber, 1997] and GRU [Cho et al., 2014a] are recurrent architectures that tackle vanishing gradient problems by incorporating gating mechanisms. They have demonstrated outstanding performance in tasks such as speech recognition [Graves et al., 2013] and neural machine translation [Sutskever et al., 2014]. Several variants of quantized LSTM and GRU have been studied in the literature (see Section 2.2).

Recently, Transformer architectures [Vaswani et al., 2017] have shown great performance even for long sequences. However, they require large training sets and exhibit a computational complexity that increases quadratically with the length of the sequence during inference. Several contributions [Prato et al., 2020, Chung et al., 2020] have demonstrated that quantization strategies are possible.

ORNN (and URNN) are known to achieve superior performance compared to LSTM in handling time series with long-term dependencies [Arjovsky et al., 2016]. They explicitly address the issues of vanishing and exploding gradients by imposing orthogonality (and unitary) constraints on the recurrent weight matrix of a vanilla RNN (See Section 2.1). As a bonus, a standard ORNN unit contains about four times fewer parameters than an LSTM unit.

To the best of our knowledge, quantization of ORNN has not been previously investigated. These are the reasons why, in this paper, we focus on quantized ORNN ⁴.

QORNN are hard to train: We emphasize that quantizing vanilla RNN and ORNN is challenging. It is identified as an open unstable problem in [Ott et al., 2016, Hou et al., 2017, Hubara et al., 2018]. The instability can be attributed to the following phenomena:

- The recurrent weight matrix is applied multiple times, rendering the network’s output highly sensitive to even slight variations in the recurrent weight matrix.
- The quantization of an orthogonal recurrent weight matrix generally results in a matrix that is not orthogonal. This, too, can contribute to the instability of the RNN.

⁴Given that ORNNs achieve comparable performance to URNN [Mhammedi et al., 2017], in the scope of lower complexity, we limit this study to ORNN

Let us illustrate the first point in Figure 1-(Left): We present in Figure 1-(Left) the values of $\frac{\|W^p - q_k(W)^p\|_F}{\|W^p\|_F}$ for different bitwidths k and various p -th power⁵ of the matrices. Here, $\|\cdot\|_F$ represents the Frobenius norm, $W \in \mathbb{R}^{10 \times 10}$ is a random matrix sampled according to a uniform law over square orthogonal matrices of size 10×10 , q_k is the quantization described in Section 3, and $p \in \{1, 10, 100, 200\}$. On Figure 1-(Left), we see that $q_k(W)^p$ can be far from W^p , especially for small bitwidths k and large values of p . As a result of this instability, the results of the forward pass using the quantized recurrent weights are far from the results for the full-precision recurrent weights, which may pose challenges in learning the quantized recurrent weights.

We illustrate the second point in Figure 1-(Right): We present boxplots of the ratio $\sigma_{\min}(q_k(W))/\sigma_{\max}(q_k(W))$, where $\sigma_{\min}(q_k(W))$ and $\sigma_{\max}(q_k(W))$ are respectively the smallest and largest singular values of $q_k(W)$. We uniformly sample 1000 orthogonal matrices W as described above, apply the quantizer q_k to each of them for different bitwidths k , and compute the ratio $\sigma_{\min}(q_k(W))/\sigma_{\max}(q_k(W))$. A ratio closer to 1 indicates a higher level of orthogonality. The boxplots show that smaller bitwidths result in smaller expected ratios and more variable ratios.

As we will see, these two sources of instability make it very challenging to achieve efficient low-bit QORNNs.

Contribution: This paper presents pioneering work in the exploration of the quantization of Orthogonal Recurrent Neural Networks (ORNN). Our main contributions can be summarized as follows:

- We investigate the factors influencing the impact of quantization on orthogonality and the behavior of ORNNs.
- We describe and empirically compare four different learning strategies for constructing Quantized and approximately Orthogonal Recurrent Neural Networks (QORNN). The most efficient strategy is a Quantization-Aware Training (QAT) algorithm that applies an orthogonal projection to full-precision weights first, followed by quantization, and is optimized using the Straight-Through Estimator (STE).
- We showcase the viability of QORNNs by empirically establishing that a QORNN, using 5 bits only, can successfully learn long-term dependencies in benchmark tasks such as the adding task and the copy task. We achieve state-of-the-art results on the permuted pixel-by-pixel MNIST (pMNIST) task, even with 3-bit quantization.

Organization of the paper: We discuss articles related to ORNNs and the quantization of vanilla RNNs in Sections 2.1 and 2.2, respectively. The notation and technical descriptions related to vanilla RNNs, orthogonality, and quantization are presented in Sections 3.1, 3.2, and 3.3, respectively. Bounds on the orthogonality discrepancy of the quantization of orthogonal matrices are provided in Section 3.4. The four algorithms for building QORNNs are detailed in Section 4. Finally, experiments and their results are presented in Section 5. Additional details can be found in the appendices. The code implementing the experiments is available at **ANONYMIZED**.

2 Related works

2.1 URNNs and ORNNs

Learning the unitary and orthogonal recurrent weight matrix of recurrent neural networks has a rich history of study in the last decade. We describe the contributions in chronological order of publication. Unitary recurrent neural networks were introduced in [Arjovsky et al., 2016]. In this article, the recurrent weight matrix is the product of parameterized unitary matrices of predefined structures. They argue empirically that URNNs are beneficial because they better capture long-term dependencies than LSTMs. Soon after, the authors of [Wisdom et al., 2016] use the *Cayley transform locally* to build an iterative scheme capable of reaching all unitary matrices. In [Jing et al., 2017], the authors parameterize the recurrent weight matrix as a product of *Givens rotations* and a diagonal matrix. By doing so, they achieve more efficient models with tunable complexity that can be trained more rapidly. In [Mhammedi et al., 2017], the authors parameterize the recurrent weight matrix as a product of *Householder reflections* to reduce the complexity of full-capacity models. In the same line of research, the authors of [Jose et al., 2018] explore the use of *product of unitary Kronecker matrices*. They incorporate a soft-orthogonality penalization term to enforce the unitary constraints. The Kronecker architecture can be adjusted to reduce the complexity of the model. In [Vorontsov et al., 2017], the authors compare soft and hard-orthogonality constraints. They find that the parameter of the soft-orthogonality strategy under study can be tuned to achieve an approximately orthogonal recurrent matrix, leading to improved efficiency. In [Helfrich et al., 2018], the authors narrow their focus to orthogonal recurrent weight matrices and parameterize the entire Stiefel manifold using the *Cayley transform scaled by a diagonal and orthogonal matrix*. Similar to [Mhammedi et al., 2017], the number of parameters defining the orthogonal matrix is optimal. In [Lezcano-Casado and Martínez-Rubio, 2019], the authors

⁵The analysis made in this paragraph does not take into account the effect of the activation function of the RNN.

parameterize orthogonal matrices using the *exponential map*. Finally, in [Kiani et al., 2022], the authors develop two Riemannian optimization strategies. The first one is based on the *orthogonal projection onto the Unitary or Stiefel manifold*, and the other on *Riemannian geodesic shooting*. The algorithms are named ProjUNN, and one of them is employed in the presented work. This choice is motivated by the experiments outlined in [Kiani et al., 2022].

2.2 Quantized RNNs

As mentioned earlier, the quantization of RNNs has been recognized as an open problem since 2016 [Ott et al., 2016]. In this article, the authors argue that quantizing vanilla RNNs is unstable. In this article, the authors only report experiments on exponential quantization for next character prediction tasks on Penn TreeBank and text8 datasets. The instability problem is also reported in [Hou et al., 2017, Hubara et al., 2018]. To the best of our knowledge, these articles are the only ones addressing the quantization of RNNs.

There are numerous studies on the quantization of LSTM, GRU, BERT, and transformers [Gupta and Agrawal, 2022, Zhu et al., 2023]. The proposals differ in various aspects, including the quantization scheme, the optimization strategy, and the quantization of the activation function.

3 Preliminaries and notations

In this section, we provide the main ideas and notations used on the RNN architecture, orthogonality, and quantization.

3.1 Vanilla RNNs

Vanilla RNNs define functions that take a time series as input and produce a vector (in the many-to-one case) or a time series (in the many-to-many case) as outputs.

In order to define them, we consider positive integers n_i and T , and an input time series $(x_t)_{t=1}^T \in (\mathbb{R}^{n_i})^T$ of length T , made of n_i -dimensional data points. Denoting the output size $n_o \in \mathbb{N}$, the output is either a vector in \mathbb{R}^{n_o} or a time series in $(\mathbb{R}^{n_o})^T$.

The architecture of the RNN is defined by a hidden layer size $n_h \in \mathbb{N}$, an activation function σ and an output activation function σ_o . The parameters defining the vanilla RNN are (W, U, V, b_o) for a recurrent weight matrix $W \in \mathbb{R}^{n_h \times n_h}$, an input-to-hidden matrix $U \in \mathbb{R}^{n_h \times n_i}$, a hidden-to-output matrix $V \in \mathbb{R}^{n_o \times n_h}$, and bias $b_o \in \mathbb{R}^{n_o}$. The hidden-state is initialized with $h_0 = 0$ and then computed using

$$h_t = \sigma(W h_{t-1} + U x_t) \in \mathbb{R}^{n_h}, \quad (1)$$

for $t \in \llbracket 1, T \rrbracket$.

In the many-to-one case, the output of the vanilla RNN is

$$\sigma_o(V h_T + b_o) \in \mathbb{R}^{n_o}.$$

In the many-to-many case, the output of the vanilla RNN is

$$\left(\sigma_o(V h_t + b_o) \right)_{t \in \llbracket 1, T \rrbracket} \in (\mathbb{R}^{n_o})^T.$$

In all the experiments, σ is either the ReLU or the modReLU [Helfrich et al., 2018] activation functions, σ_o is the identity function for regression tasks and the softmax function for classification tasks. The parameters (W, U, V, b_o) are learned and W is constrained to be quantized and approximately orthogonal. The matrix U is also quantized.

3.2 Orthogonality

The matrix $W \in \mathbb{R}^{n_h \times n_h}$ is orthogonal if and only if

$$W'W = WW' = I,$$

where I denotes the identity matrix in $\mathbb{R}^{n_h \times n_h}$ and W' is the transpose of W . This necessitates that the columns (respectively, rows) of the matrix possess a Euclidean norm of 1, with the additional condition that any two distinct columns (respectively, rows) exhibit a scalar product of 0. Among the various properties of orthogonal matrices, it is important to note that the singular values of orthogonal matrices are all equal to 1. Denoting $\sigma_{\min}(W)$ and $\sigma_{\max}(W)$ as the smallest and largest singular values of W , we have $\sigma_{\min}(W) = \sigma_{\max}(W) = 1$. In other words, multiplication by an

orthogonal matrix preserves norms. Orthogonal matrices constitute the Stiefel manifold [Edelman et al., 1998] that we denote $St(n_h)$.

The motivation for constraining the recurrent weight matrix to be orthogonal has been discussed in numerous articles. We reiterate it for completeness in Appendix A.

As is common, we distinguish between *hard orthogonality* and *soft orthogonality*. In the models described in Section Section 4, we utilize tools from both of these categories.

Soft-orthogonality The typical strategy for soft orthogonality involves adding a regularization term to the learning objective L . An effective example of such a regularization term is

$$R(W) = \|WW' - I\|_F^2, \quad (2)$$

where $\|\cdot\|_F$ denotes the Frobenius norm. Depending on the value of the parameter that balances L and R , orthogonality is enforced more or less strictly.

Hard-orthogonality Hard orthogonality strategies rigorously impose W to be orthogonal. We consider two such strategies. Both strategies establish a mapping from $\mathbb{R}^{n_h \times n_h}$ to $St(n_h)$.

- **projUNN:** The first strategy employs the mapping P_{projUNN} as defined and implemented, referred to as projUNN-D, in [Kiani et al., 2022]. This mapping computes the image $P_{\text{projUNN}}(W)$ of matrix W as the nearest orthogonal matrix in terms of the Frobenius norm. The implementation relies on a closed-form expression derived in [Keller, 1975]. In the sequel, we use P_{projUNN} to implement a projected gradient descent algorithm solving a minimization problem involving an orthogonality constraint.
- **Björck:** The second strategy apply a fixed and sufficiently large number of iterations of the gradient descent algorithm minimizing R [Björck and Bowie, 1971, Anil et al., 2019] (more details in Appendix B). The resulting mapping from $\mathbb{R}^{n_h \times n_h}$ to the Stiefel manifold $St(n_h)$, denoted as $P_{\text{Björck}}$, is surjective. Therefore, minimizing $L(P_{\text{Björck}}(W))$ among unconstrained W is equivalent to minimizing $L(W)$ among orthogonal W .

Notice that standard backpropagation permits to compute $\left. \frac{\partial L \circ P_{\text{Björck}}}{\partial W} \right|_W$.

3.3 Quantization

We consider in this paper the most common scheme of quantization: a uniform quantization with a scaling parameter [Rastegari et al., 2016, Gholami et al., 2022]. For a quantization of bitwidth k , where $k \geq 2$, the set of possible values is restricted to a set of size 2^k , defined for a given $\alpha > 0$, as follows:

$$\mathcal{Q}_k = \frac{\alpha}{2^{k-1}} \left[-2^{k-1}, 2^{k-1} - 1 \right].$$

The set \mathcal{Q}_k evenly distributes values between $-\alpha$ and $\alpha - \frac{\alpha}{2^{k-1}}$, with a quantization step of $\frac{\alpha}{2^{k-1}}$.

For given k and α , the quantizer q_k maps every $W \in \mathbb{R}^{n_h \times n_h}$ to the nearest element in $\mathcal{Q}_k^{n_h \times n_h}$ based on the Frobenius norm⁶. In other words, for every $(i, j) \in \llbracket 1, n_h \rrbracket^2$, the entry (i, j) of the matrix $q_k(W)$, denoted $(q_k(W))_{i,j}$, is the nearest element in \mathcal{Q}_k to $W_{i,j}$.

All considered quantizers take the value $\alpha = \|W\|_{\max}$, where $\|W\|_{\max} = \max_{i,j} |W_{ij}|$. For ease of notation, we do not explicitly express the dependence on α . Note that, as is common practice [Rastegari et al., 2016], when minimizing a function involving $q_k(W)$ with respect to W , we treat α as a constant. Consequently, we do not backpropagate the gradient with respect to α . To backpropagate through q_k , we employ the classical Straight-Through-Estimator (STE), described for completeness in Appendix C.

3.4 Inducing approximate orthogonality to $q_k(W)$

It is worth noting that, even when W is orthogonal, the output $q_k(W)$ of the quantizer is generally not orthogonal. Research on Hadamard matrices suggests, in large dimensions, the difficulty of finding matrices that are both quantized and orthogonal [Horadam, 2012, Hedayat and Wallis, 1978]. We anticipate that there is no direct method to obtain a matrix close to W that is both quantized and orthogonal.

⁶Note that this paper only consider weight quantization since it has the largest influence on convergence.

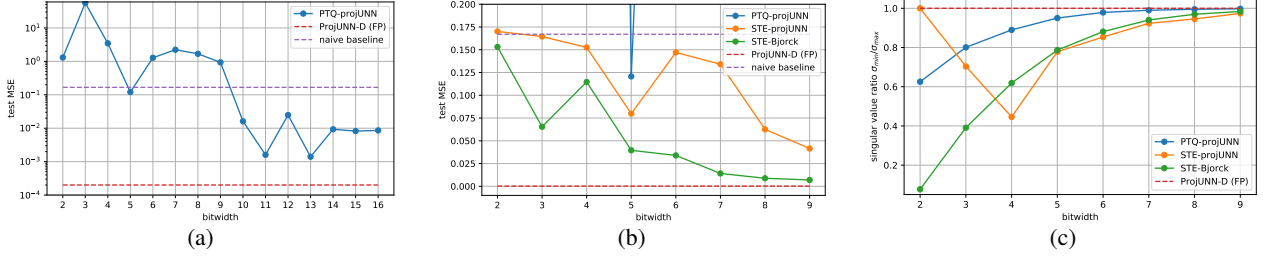


Figure 2: Adding task experiments for $T = 750$, several quantization bitwidths k , and $n_h = 170$: (a) PTQ-projUNN test error; (b) STE-projUNN, STE-Bjorck and projUNN (FP) test errors. LSTM (FP) test errors are identical to those of projUNN (FP); (c) Ratio $\sigma_{\min}(W_q)/\sigma_{\max}(W_q)$.

As expressed by the bounds calculated below in (3) and (4), when W is orthogonal, if k is large enough, we expect $W_q = q_k(W)$ to remain close to orthogonality. However, these bounds provide satisfactory guarantees only when $n_h \ll 2^{k-1}$. Unfortunately, this condition is not met in the scenarios of interest. While we will observe in the experiments that it works in practice, the worst-case bounds do not guarantee that imposing orthogonality on W will result in a quantized matrix $q_k(W)$ that is sufficiently close to orthogonality.

Evaluating the approximate orthogonality of $q_k(W)$ Assume W is orthogonal and denote $H = W_q - W$, where $W_q = q_k(W)$. Since W is orthogonal, we have $\|WH'\|_F = \|H'\|_F = \|H\|_F$, and we obtain:

$$\begin{aligned} \|W_q W_q' - I\|_F &= \|(W + H)(W + H)' - WW'\|_F \\ &= \|WH' + HW' + HH'\|_F \\ &\leq 2\|WH'\|_F + \|HH'\|_F \\ &\leq 2\|H\|_F + \|H\|_F^2. \end{aligned}$$

Considering that, with the quantization scheme defined in Section 3.3, we have $\|H\|_{\max} \leq \frac{\alpha}{2^{k-1}} = \frac{\|W\|_{\max}}{2^{k-1}}$ and noting that, since W is orthogonal, $\|W\|_{\max} \leq 1$, we have the inequalities $\|H\|_F \leq n_h \|H\|_{\max} \leq \frac{n_h}{2^{k-1}}$. This leads to

$$\|W_q W_q' - I\|_F \leq 2 \frac{n_h}{2^{k-1}} + \left(\frac{n_h}{2^{k-1}} \right)^2. \quad (3)$$

Similarly, using that $\sigma_{\max}(H) \leq n_h \|H\|_{\max} \leq \frac{n_h}{2^{k-1}}$ and that W is orthogonal, we obtain

$$1 - \frac{n_h}{2^{k-1}} \leq \sigma_{\min}(W_q) \quad \text{and} \quad \sigma_{\max}(W_q) \leq 1 + \frac{n_h}{2^{k-1}}. \quad (4)$$

4 Quantized RNNs with approximate orthogonality constraints

In this section, we describe the four proposed strategies to build QORNN that are evaluated in Section 5. Each strategy is presented in one of the following subsections.

4.1 Post-Training Quantization (PTQ-projUNN)

For all values of k , the weights with approximate orthogonality constraints, and quantized using k bits, are $(q_k(W), q_k(U), V, b_o)$, where (W, U, V, b_o) is the full-precision parameters obtained using the *projUNN-D* algorithm [Kiani et al., 2022] for solving

$$\begin{cases} \min_{(W, U, V, b_o)} L(W, U, V, b_o) \\ W \text{ is orthogonal,} \end{cases}$$

where L is the learning objective.

4.2 Penalized STE (STE-pen)

A Quantized-Aware-Training (QAT) strategy is applied to directly learn quantized weights with approximate orthogonality constraints $(q_k(W), q_k(U), V, b_o)$, for a given k . (W, U, V, b_o) are obtained using an implementation of the

Straight-Through Estimator (STE) to solve the following optimization problem:

$$\min_{(W,U,V,b_o)} L(q_k(W), q_k(U), V, b_o) + \lambda R(q_k(W)). \quad (5)$$

Here, L represents the learning objective, R is the regularization term enforcing orthogonality as defined in (2), and λ is a parameter that balances the trade-off between minimizing L and R . A similar model has been tested for vision tasks in [Eryilmaz and Dundar, 2023]. Results of experiments with another regularization term are reported in Appendix D.

4.3 Projected STE (STE-projUNN)

A QAT strategy is applied to directly learn quantized weights with approximate orthogonality constraints $(q_k(W), q_k(U), V, b_o)$, for a given k . (W, U, V, b_o) are obtained using ProjUNN-D *projected gradient descent algorithm* solving the following optimization problem:

$$\begin{cases} \min_{(W,U,V,b_o)} L(q_k(W), q_k(U), V, b_o) \\ W \text{ is orthogonal,} \end{cases} \quad (6)$$

where L is the learning objective. In the projected gradient descent algorithm, the gradients are computed using backpropagation and the STE, and the projections onto the Stiefel manifold are computed using P_{projUNN} .

4.4 STE with $P_{\text{Björck}}$ (STE-Björck)

A QAT strategy is applied to directly learn quantized weights with approximate orthogonality constraints $(q_k(P_{\text{Björck}}(W)), q_k(U), V, b_o)$, for a given k . Inspired by [Anil et al., 2019], (W, U, V, b_o) are obtained using the differentiable surjective mapping onto the Stiefel manifold $P_{\text{Björck}}$, and solve the optimization problem:

$$\min_{(W,U,V,b_o)} L(q_k(P_{\text{Björck}}(W)), q_k(U), V, b_o),$$

where L is the learning objective. As already explained, since $P_{\text{Björck}}$ is surjective onto the Stiefel manifold, solving this problem is equivalent to solving (6). However, the reformulation leads to a different algorithm. The gradients are also computed using backpropagation and the STE.

5 Experiments

In this section, we present the results of the models described in Section 4 on several standard sequential tasks: the adding task in Section 5.1, the copy task in Section 5.2, the permuted pixel-by-pixel MNIST (pMNIST) task in Section 5.3, and the next character prediction for the Penn TreeBank dataset in Section 5.4. Three of these tasks are designed to be challenging because they rely on long-term dependencies within the sequences, making them well-suited for ORNNs. The fourth task pertains to a language model problem characterized by shorter-term dependencies.

To assess the performance of the QORNN, we also provide, in Section 5.1, 5.2, 5.3, and 5.4, the performances of two full-precision RNNs:

- LSTM [Hochreiter and Schmidhuber, 1997] of the same hidden size as the quantized models (except for Penn TreeBank, see Section 5.4), referred to as *LSTM (FP)*.
- ORNNs of the same hidden size as the quantized models, obtained using the projUNN-D algorithm [Kiani et al., 2022], referred to as *projUNN-D (FP)*.

Additionally, we include the performance corresponding to random guessing, referred to as the *naive baseline*.

As recommended in [Kiani et al., 2022], we utilize the RMSprop optimizer for training ProjUNN-D. The classical Adam optimizer [Kingma and Ba, 2015] is employed for all other models. Additional parameters can be found in Appendix E to H.

5.1 Adding task

We consider the Adding task as described in [Arjovsky et al., 2016]. In this task, the input to the RNN is a time series $(x_t)_{t=1}^T \in (\mathbb{R}^2)^T$. Denoting for all t , $x_t = (x[0]_t, x[1]_t)$, $(x[0]_t)_{t=1}^T$ consists of random scalars sampled independently and uniformly from the interval $[0, 1]$, while $(x[1]_t)_{t=1}^T$ consists of zeros except for two randomly selected entries set to

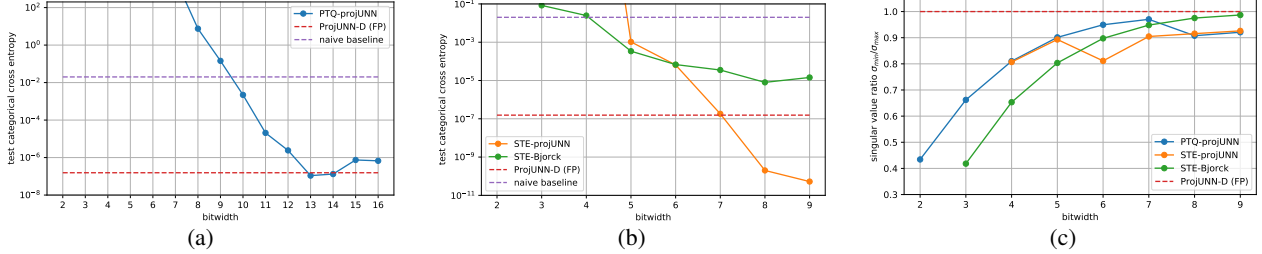


Figure 3: Copy task experiments for $T = 1000 + 20$, several quantization bitwidths k , and $n_h = 256$: (a) PTQ-projUNN test error; (b) STE-projUNN, STE-Bjorck and projUNN test errors. As reported in [Wisdom et al., 2016], LSTM (FP) settles for the naive baseline; (c) Ratio $\sigma_{\min}(W_q)/\sigma_{\max}(W_q)$.

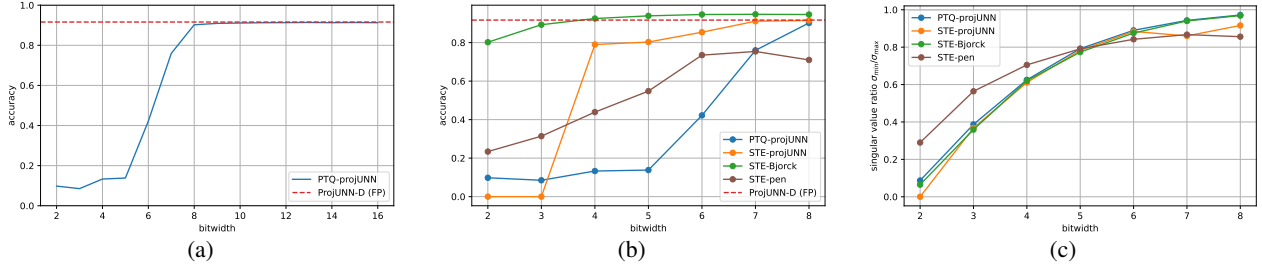


Figure 4: pMNIST experiments for several quantization bitwidths k , and $n_h = 170$: (a) PTQ-projUNN test accuracy; (b) Test accuracy for all approaches. LSTM (FP) test accuracy is identical to that of projUNN (FP); (c) Ratio $\sigma_{\min}(W_q)/\sigma_{\max}(W_q)$.

1. The output is $\sum_t x[0]_t \cdot x[1]_t$. As T increases, this task evolves into a problem that requires longer-term memory. The naive baseline mean squared error (MSE) is approximately 0.167. More details are given in Appendix E.

We follow [Helfrich et al., 2018] for most settings and consider $T = 750$, and $n_h = 170$. Learning curves and results for $n_h = 400$ are described in the Appendix E, leading to similar conclusions. The activation function σ is the Rectified Linear Unit (ReLU), and σ_o is the identity. The recurrent weight matrix is initialized to the identity matrix I . We performed experiments for each of the four proposed strategies– PTQ-projUNN, STE-pen, STE-projUNN, and STE-Bjorck – and for every $k \in [2, 9]$.

Note that, when learning with projUNN, the recurrent weight matrix remains very close to the identity during the learning process. Since the quantization of such matrices would result in reverting to the identity matrix, we have modified the quantization scheme for this experiment and the PTQ-projUNN and STE-projUNN strategies. The quantized matrix is defined as $W_q = I + q_k(W - I)$.

Confirming the challenging and unstable nature of quantizing ORNNs [Ott et al., 2016, Hubara et al., 2018, Hou et al., 2017], Figure 2-a illustrates that PTQ-projUNN is only feasible for a large bitwidth, $k \geq 10$.

The STE-pen method fails to learn, regardless of the bitwidth. In Figure 2-b, we observe that both STE-Bjorck and STE-projUNN successfully learn the task, achieving a lower MSE than the naive baseline, even with only 2 or 3 bits. However, the STE-projUNN strategy is more challenging to learn than STE-Bjorck. This is possibly due to the resulting matrices being close to the identity.

Since the orthogonal property is essential for learning long-term dependencies, we examine the ratio between the minimum and maximum singular values of W_q in Figure 2-c. Astonishingly, STE-Bjorck is able to initiate learning for this task with a low ratio. However, as expected, achieving more precise learning involves matrices that are close to orthogonal, i.e. for bitwidths $k \geq 5$.

5.2 Copy task

We build RNNs solving the copy task as described in [Wisdom et al., 2016], based on the setup outlined by [Hochreiter and Schmidhuber, 1997]. This task is known to be a difficult long-term memory benchmark, that classical LSTMs struggle to solve [Wisdom et al., 2016, Helfrich et al., 2018]. The input is a sequence of length $T = T_0 + 20$, where the initial 10 elements constitute a sequence for the network to memorize, followed by a marker at $T_0 + 11$.

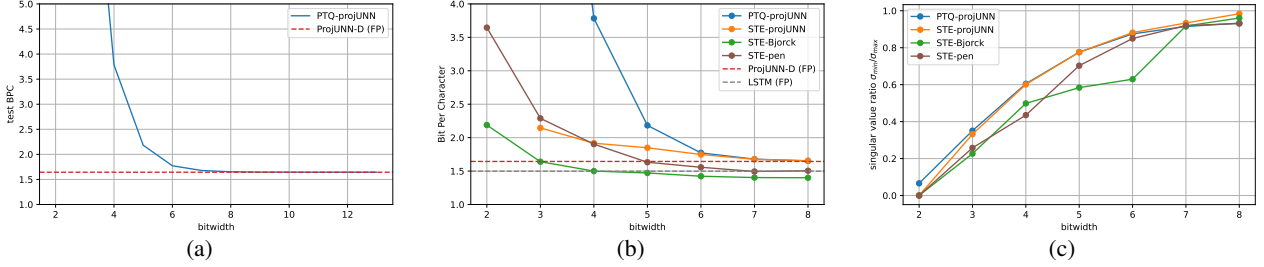


Figure 5: Penn TreeBank experiments for several quantization bitwidths k , and $n_h = 1024$: (a) PTQ-projUNN BPC; (b) BPC for all approaches. LSTM (FP) is given for a hidden size of 256, yielding better results; (c) Ratio $\sigma_{\min}(W_q)/\sigma_{\max}(W_q)$.

The RNN’s objective is to generate a sequence of the same length, with the last ten elements replicating the initial 10 elements of the input sequence. More details are given in Appendix F.

The output activation σ_o is the softmax, and the prediction error is measured using the average cross-entropy. The naive baseline has an expected cross-entropy of $\frac{10 \log 8}{T_0+20}$.

As in [Kiani et al., 2022], we conducted the experiments for $T_0 = 1000$ timesteps, with ORNNs of size $n_h = 256$. Details on the hyperparameters, learning curves, results for $n_h = 190$ and $T_0 = 2000$ are provided in the Appendix F.

All the results are on Figure 3. The performance of projUNN (FP) is significantly degraded by PTQ-projUNN for $k \leq 9$. STE-pen also fails to learn, regardless of the bitwidth. As reported by [Wisdom et al., 2016], LSTM also remains stuck at the naive baseline. Both STE-projUNN and STE-Bjorck require $k \geq 5$ to converge (Y-axis in Figure 3-b is in log scale). We observe in Figure 3-c that the conditioning of the quantized recurrent weight matrix has a direct impact on the performance of the STE-projUNN and STE-Bjorck. A good conditioning is not sufficient for PTQ-projUNN.

5.3 Permuted pixel-by-pixel MNIST (pMNIST)

This task is also considered a challenging long-term memory problem. Here, data examples are the 28×28 images from the MNIST dataset, where each image is flattened to a 784-long sequence of 1-dimensional pixels (normalized values in $[0, 1]$), and the pixels are randomly shuffled according to a fixed permutation. The model has to predict the hand-written digit class (10 outputs).

In this section, we fix $n_h = 170$ for all algorithms. Results for STE-pen with another regularization term are in the Appendix D. We use the ReLU activation with the STE-pen and STE-Bjorck strategies, and as recommended in [Kiani et al., 2022] the modReLU activation with the STE-projUNN, projUNN (FP) and PTQ-projUNN strategies (see Appendix G for details). For each algorithm, we test all bitwidths $k \in \llbracket 2, 8 \rrbracket$. We measure performances using the accuracy and compare the results with those of LSTM (FP): a trained LSTM with a hidden size of $n_h = 170$ and full-precision weights.

For STE-pen, mere quantization of the recurrent weight matrix leads to significant spectral norm alteration, hindering the learning process. To avoid this problem, we found it useful to normalize the matrix by its spectral norm after each quantization step.

In Figure 4-b, we observe that STE-Bjorck outperforms all other strategies for all bitwidths, and yields better results than the LSTM (FP) and projUNN (FP) even for small bitwidths ($k \geq 4$). As for the Adding task, STE-Bjorck is able to learn significant information (accuracy ≥ 0.8), even when the condition number is small ($\sigma_{\min}(W_q)/\sigma_{\max}(W_q) \leq 0.5$, Figure 4-c). For $k \geq 5$, STE-Bjorck achieves results comparable to those reported in [Lezcano-Casado and Martínez-Rubio, 2019, Kiani et al., 2022], which currently represent the state-of-the-art in orthogonal and unitary recurrent networks. We observe that the STE-projUNN strategy produces results similar to projUNN-D (FP) and LSTM (FP), though requiring a bitwidth of 7 or more, which corresponds to a high orthogonality level ($\sigma_{\min}(W_q)/\sigma_{\max}(W_q) \geq 0.8$). Again, the PTQ-projUNN approach only matches the performance of projUNN-D (FP) and LSTM (FP) for bitwidths $k \geq 8$, confirming the difficulty of ORNN quantization. The STE-pen approach never achieves 80% accuracy.

5.4 Character level Penn TreeBank

We provide results of QORNNs on a language modeling task. The Penn TreeBank dataset [Marcus et al., 1993] (PTB) is a corpus of sentences of 50 different characters. The goal of the task is to predict the next character based on the preceding ones (further details can be found in Appendix H).

All experiments described in this section are for $n_h = 1024$, except for LSTM (FP) for which we set $n_h = 256$ to avoid overfitting. Again, our learning approaches are tested for all bitwidths $k \in \llbracket 2, 8 \rrbracket$. The models are evaluated with the Bit Per Character measure (BPC).

The results for this task are reported in Figure 5. The STE-Bjorck approach allows beating LSTM (FP) for small bitwidths ($k \geq 4$). The STE-projUNN achieves similar performances as projUNN (FP) for $k = 8$. Interestingly, this task is the only one for which STE-pen comes close to the LSTM (FP) for $k = 7$ and $k = 8$. This could be attributed to the task not relying on dependencies over an extended delay compared to the others. PTQ-projUNN reaches results comparable to the full-precision version only for $k \geq 8$.

6 Conclusion and perspectives

In this paper, we examined the impact of bitwidth in the quantization of ORNNs using four QAT and PTQ approaches, demonstrating empirically the advantages of using QAT methods over PTQ. The proposed STE-Bjorck approach, described in Section 4.4, demonstrates compelling performance even for small bitwidths, paving the way for the resource-efficient implementation of approximately orthogonal RNNs and prompting a more in-depth analysis.

Future work on QORNNs could therefore focus on developing alternative learning approaches and quantization schemes, creating methods for quantizing both weights and activations, and implementing them on dedicated hardware.

Acknowledgments and Disclosure of Funding

This work has benefited from the AI Interdisciplinary Institute ANITI, which is funded by the French “Investing for the Future – PIA3” program under the Grant agreement ANR-19-P3IA-0004. The authors gratefully acknowledge the support of the DEEL project.⁷

References

- [Anil et al., 2019] Anil, C., Lucas, J., and Grosse, R. (2019). Sorting out Lipschitz function approximation. In *International Conference on Machine Learning*, pages 291–301. PMLR.
- [Arjovsky et al., 2016] Arjovsky, M., Shah, A., and Bengio, Y. (2016). Unitary evolution recurrent neural networks. In *International Conference on Machine Learning*, pages 1120–1128. PMLR.
- [Bengio et al., 2013] Bengio, Y., Léonard, N., and Courville, A. (2013). Estimating or propagating gradients through stochastic neurons for conditional computation. *arXiv preprint arXiv:1308.3432*.
- [Bengio et al., 1994] Bengio, Y., Simard, P., and Frasconi, P. (1994). Learning long-term dependencies with gradient descent is difficult. *IEEE Transactions on Neural Networks*, 5(2):157–166.
- [Björck and Bowie, 1971] Björck, Å. and Bowie, C. (1971). An iterative algorithm for computing the best estimate of an orthogonal matrix. *SIAM Journal on Numerical Analysis*, 8(2):358–364.
- [Cho et al., 2014a] Cho, K., van Merriënboer, B., Bahdanau, D., and Bengio, Y. (2014a). On the properties of neural machine translation: encoder–decoder approaches. In *Proceedings of the 8th Workshop on Syntax, Semantics and Structure in Statistical Translation*, pages 103–111.
- [Cho et al., 2014b] Cho, K., van Merriënboer, B., Gulcehre, C., Bahdanau, D., Bougares, F., Schwenk, H., and Bengio, Y. (2014b). Learning phrase representations using RNN encoder–decoder for statistical machine translation. In *Proceedings of the Conference on Empirical Methods in Natural Language Processing*, page 1724.
- [Chung et al., 2020] Chung, I., Kim, B., Choi, Y., Kwon, S. J., Jeon, Y., Park, B., Kim, S., and Lee, D. (2020). Extremely low bit transformer quantization for on-device neural machine translation. In *Findings of the Association for Computational Linguistics: EMNLP 2020*, pages 4812–4826.
- [Courbariaux et al., 2015] Courbariaux, M., Bengio, Y., and David, J.-P. (2015). BinaryConnect: Training deep neural networks with binary weights during propagations. *Advances in Neural Information Processing Systems*, 28.

⁷<https://www.deel.ai/>

- [Edelman et al., 1998] Edelman, A., Arias, T. A., and Smith, S. T. (1998). The geometry of algorithms with orthogonality constraints. *SIAM journal on Matrix Analysis and Applications*, 20(2):303–353.
- [Eryilmaz and Dunder, 2023] Eryilmaz, S. B. and Dunder, A. (2023). Understanding how orthogonality of parameters improves quantization of neural networks. *IEEE Transactions on Neural Networks and Learning Systems*, 34(12):10737–10746.
- [Gholami et al., 2022] Gholami, A., Kim, S., Zhen, D., Yao, Z., Mahoney, M., and Keutzer, K. (2022). A survey of quantization methods for efficient neural network inference. In *Low-Power Computer Vision*, chapter 13, pages 291–326. Chapman and Hall/CRC.
- [Graves et al., 2013] Graves, A., Mohamed, A.-r., and Hinton, G. (2013). Speech recognition with deep recurrent neural networks. In *IEEE International Conference on Acoustics, Speech and Signal Processing*, pages 6645–6649. IEEE.
- [Gupta and Agrawal, 2022] Gupta, M. and Agrawal, P. (2022). Compression of deep learning models for text: A survey. *ACM Transactions on Knowledge Discovery from Data (TKDD)*, 16(4):1–55.
- [Hedayat and Wallis, 1978] Hedayat, A. and Wallis, W. D. (1978). Hadamard matrices and their applications. *The Annals of Statistics*, 6(6):1184–1238.
- [Helfrich et al., 2018] Helfrich, K., Willmott, D., and Ye, Q. (2018). Orthogonal recurrent neural networks with scaled Cayley transform. In *International Conference on Machine Learning*, pages 1969–1978. PMLR.
- [Henaff et al., 2016] Henaff, M., Szlam, A., and LeCun, Y. (2016). Recurrent orthogonal networks and long-memory tasks. In *International Conference on Machine Learning*, pages 2034–2042. PMLR.
- [Hinton, 2012] Hinton, G. (2012). Neural networks for machine learning. Coursera, video lectures. Lecture 15b.
- [Hochreiter and Schmidhuber, 1997] Hochreiter, S. and Schmidhuber, J. (1997). Long short-term memory. *Neural computation*, 9(8):1735–1780.
- [Horadam, 2012] Horadam, K. J. (2012). *Hadamard matrices and their applications*. Princeton university press.
- [Hou et al., 2017] Hou, L., Yao, Q., and Kwok, J. T. Y. (2017). Loss-aware binarization of deep networks. In *International Conference on Learning Representations*.
- [Hubara et al., 2018] Hubara, I., Courbariaux, M., Soudry, D., El-Yaniv, R., and Bengio, Y. (2018). Quantized neural networks: Training neural networks with low precision weights and activations. *Journal of Machine Learning Research*, 18(187):1–30.
- [Jing et al., 2017] Jing, L., Shen, Y., Dubcek, T., Peurifoy, J., Skirlo, S., LeCun, Y., Tegmark, M., and Soljačić, M. (2017). Tunable efficient unitary neural networks (EUNN) and their application to RNNs. In *International Conference on Machine Learning*, pages 1733–1741. PMLR.
- [Jose et al., 2018] Jose, C., Cissé, M., and Fleuret, F. (2018). Kronecker recurrent units. In *International Conference on Machine Learning*, pages 2380–2389. PMLR.
- [Keller, 1975] Keller, J. B. (1975). Closest unitary, orthogonal and Hermitian operators to a given operator. *Mathematics Magazine*, 48(4):192–197.
- [Kiani et al., 2022] Kiani, B., Balestriero, R., LeCun, Y., and Lloyd, S. (2022). projUNN: efficient method for training deep networks with unitary matrices. *Advances in Neural Information Processing Systems*, 35.
- [Kingma and Ba, 2015] Kingma, D. P. and Ba, J. (2015). Adam: A method for stochastic optimization. In *International Conference on Learning Representations*.
- [Lezcano-Casado and Martínez-Rubio, 2019] Lezcano-Casado, M. and Martínez-Rubio, D. (2019). Cheap orthogonal constraints in neural networks: A simple parametrization of the orthogonal and unitary group. In *International Conference on Machine Learning*, pages 3794–3803. PMLR.
- [Marcus et al., 1993] Marcus, M. P., Santorini, B., and Marcinkiewicz, M. A. (1993). Building a large annotated corpus of English: The Penn Treebank. *Computational Linguistics*, 19(2):313–330.
- [Mhammedi et al., 2017] Mhammedi, Z., Hellicar, A. D., Rahman, A., and Bailey, J. (2017). Efficient orthogonal parametrisation of recurrent neural networks using Householder reflections. In *International Conference on Machine Learning*, pages 2401–2409. PMLR.
- [Ott et al., 2016] Ott, J., Lin, Z., Zhang, Y., Liu, S.-C., and Bengio, Y. (2016). Recurrent neural networks with limited numerical precision. *arXiv preprint arXiv:1608.06902*.
- [Prato et al., 2020] Prato, G., Charlaix, E., and Rezagholizadeh, M. (2020). Fully quantized transformer for machine translation. In *Findings of the Association for Computational Linguistics: EMNLP 2020*, pages 1–14.

- [Rastegari et al., 2016] Rastegari, M., Ordonez, V., Redmon, J., and Farhadi, A. (2016). Xnor-net: Imagenet classification using binary convolutional neural networks. In *European Conference on Computer Vision*, pages 525–542. Springer.
- [Rumelhart et al., 1986] Rumelhart, D. E., Hinton, G. E., and Williams, R. J. (1986). Learning representations by back-propagating errors. *Nature*, 323(6088):533–536.
- [Sayed et al., 2023] Sayed, R., Azmi, H., Shawkey, H. A., Khalil, A. H., and Refky, M. (2023). A systematic literature review on binary neural networks. *IEEE Access*, 11:27546–27578.
- [Sutskever et al., 2014] Sutskever, I., Vinyals, O., and Le, Q. V. (2014). Sequence to sequence learning with neural networks. *Advances in Neural Information Processing Systems*, 27.
- [Vaswani et al., 2017] Vaswani, A., Shazeer, N., Parmar, N., Uszkoreit, J., Jones, L., Gomez, A. N., Kaiser, Ł., and Polosukhin, I. (2017). Attention is all you need. *Advances in Neural Information Processing systems*, 30.
- [Vorontsov et al., 2017] Vorontsov, E., Trabelsi, C., Kadoury, S., and Pal, C. (2017). On orthogonality and learning recurrent networks with long term dependencies. In *International Conference on Machine Learning*, pages 3570–3578. PMLR.
- [Wisdom et al., 2016] Wisdom, S., Powers, T., Hershey, J., Le Roux, J., and Atlas, L. (2016). Full-capacity unitary recurrent neural networks. *Advances in Neural Information Processing Systems*, 29.
- [Yuan and Agaian, 2023] Yuan, C. and Agaian, S. S. (2023). A comprehensive review of binary neural network. *Artificial Intelligence Review*, pages 12949–13013.
- [Zhu et al., 2023] Zhu, X., Li, J., Liu, Y., Ma, C., and Wang, W. (2023). A survey on model compression for large language models. *arXiv preprint arXiv:2308.07633*.

A Memorization and stability, vanishing and exploding gradient

For a large T , if the largest singular value σ_{\max} of the weight matrix W is smaller than 1, the initial entries of the input $(x_t)_{t=1}^T$ cannot be effectively retained in the hidden state h_T . This prevents the consideration of long-term dependencies. Conversely, still considering large T , if the smallest singular value σ_{\min} of W is greater than 1, each multiplication by W in (1) increases the magnitude of h_t , and the norm $\|h_t\|$ may tend towards infinity, leading to instability. For memorization and stability issues, it is desirable for the singular values of W to remain close to 1.

We arrive at the same conclusion when attempting to mitigate issues related to vanishing and exploding gradients. As indicated in [Arjovsky et al., 2016] and echoed in subsequent literature on URNNs, denoting L the loss function, we find that:

$$\begin{aligned} \frac{\partial L}{\partial h_t} &= \frac{\partial L}{\partial h_T} \frac{\partial h_T}{\partial h_t} \\ &= \frac{\partial L}{\partial h_T} \prod_{i=t}^{T-1} \frac{\partial h_{i+1}}{\partial h_i} \\ &= \frac{\partial L}{\partial h_T} \prod_{i=t}^{T-1} D_i W', \end{aligned}$$

where $D_i = \text{diag}(\sigma'(W h_{i-1} + U x_i))$ is the Jacobian⁸ matrix of σ evaluated at the pre-activation point and W' is the transpose of W . If all the singular values of W are less than 1, those of $D_i W'$ are as well, causing the norm of $\frac{\partial L}{\partial h_t}$ to rapidly approach 0 as t decreases—resulting in the vanishing gradient problem. Conversely, if some singular values of W are greater than 1, depending on the activation patterns and $\frac{\partial L}{\partial h_T}$, the norm may explode, leading to the exploding gradient problem. To mitigate these phenomena, it is desirable for the singular values of W to remain close to 1. In other words, we aim for W to be orthogonal or at least approximately orthogonal.

B The Björck algorithm

Björck algorithm [Björck and Bowie, 1971] aims to minimize the regularization term R . As described in [Anil et al., 2019], the initialization is done with the matrix $A_0 = \frac{1}{\sigma_{\max}(W)} W$, where $\sigma_{\max}(W)$ is the largest singular value of W , computed using the power iteration for a fixed number of iterations. Then it applies a fixed and sufficiently large number of iterations, in practice 15, of the following operation:

$$A_{k+1} = A_k \left(I + \sum_{i=1}^p (-1)^i \binom{-\frac{1}{2}}{i} Q_k^i \right)$$

where $Q_k = I - A_k' A_k$ and $\binom{z}{p} = \frac{1}{p!} \prod_{i=0}^{p-1} (z - i)$. As described in [Anil et al., 2019], we take $p = 1$. In this case, the Björck algorithm corresponds to several iterations of the gradient descent algorithm minimizing R :

$$A_{k+1} = A_k - \frac{1}{2} A_k (A_k' A_k - I) = \frac{3}{2} A_k - \frac{1}{2} A_k A_k' A_k,$$

initialized at $A_0 = \frac{1}{\sigma_{\max}(W)} W$.

We compute $\left. \frac{\partial P_{\text{Björck}}}{\partial W} \right|_W$ using standard backpropagation but treat $\sigma_{\max}(W)$ as a constant.

C The straight-through-estimator

Considering α as fixed, the mapping $W \mapsto q_k(W)$ is piecewise constant. Its gradient at W , denoted as $\left. \frac{\partial q_k}{\partial W} \right|_W$, is either undefined or 0. This issue is well-known in quantization-aware training, which aim to minimize an objective

⁸Since it is not central to our article, we assume that all the entries of $W h_{i-1} + U x_i$ are non-zero, ensuring that the Jacobian and σ' are well-defined.

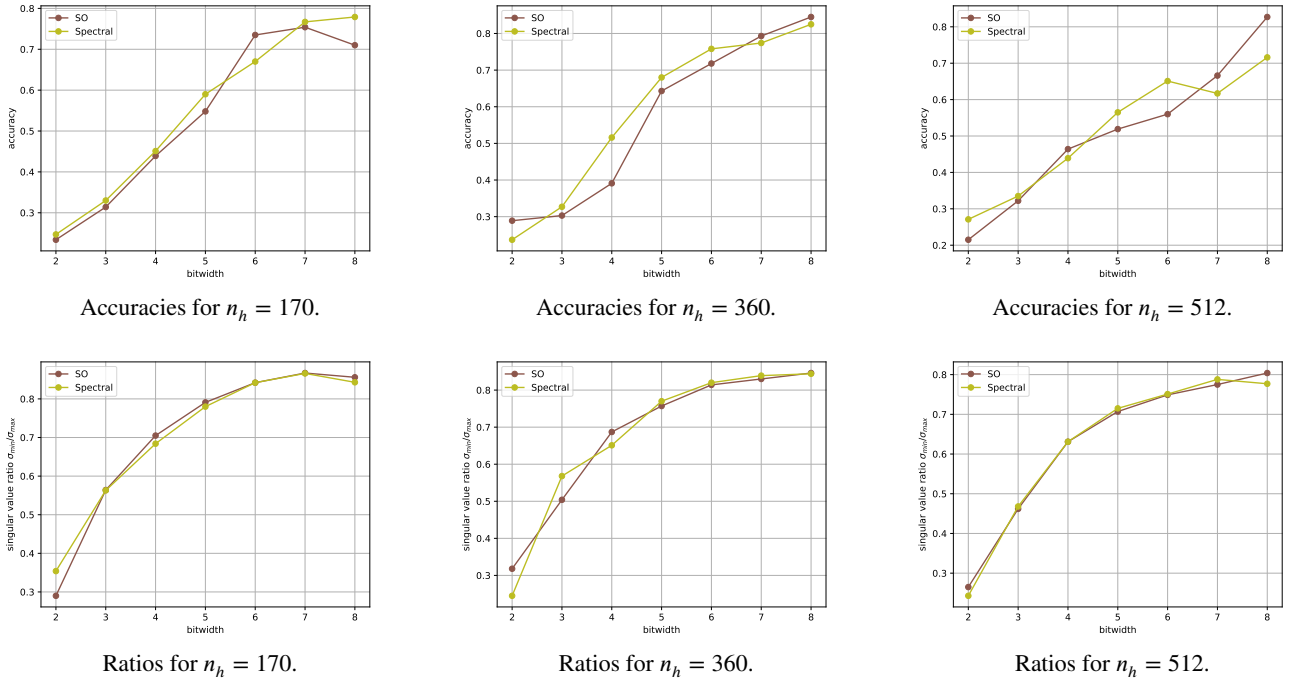


Figure 6: pMNIST: Test accuracy and ratio $\sigma_{\min}(q_k(W))/\sigma_{\max}(q_k(W))$ for STE-pen with different soft-orthogonality regularizers: ‘SO’ corresponds to the regularizer $R^{SO}(W) = \|W W' - I\|_F^2$; ‘Spectral’ corresponds to the regularizer $R^{spectral} = \sum_{i=1}^{n_h} |\sigma_i - 1|^2$.

$L(q_k(W))$ with respect to W , where $W_q \mapsto L(W_q)$ is the learning loss. Backpropagating the gradient using the chain rule

$$\frac{\partial L \circ q_k}{\partial W} \Big|_W = \frac{\partial L}{\partial W_q} \Big|_{q_k(W)} \frac{\partial q_k}{\partial W} \Big|_W$$

is either not possible or results in a null gradient in this context.

To address this issue, backpropagation through the quantizer is performed using the straight-through estimator (STE) [Hinton, 2012, Bengio et al., 2013, Courbariaux et al., 2015]. The STE approximates the gradient using

$$\frac{\partial L \circ q_k}{\partial W} \Big|_W \approx \frac{\partial L}{\partial W_q} \Big|_{q_k(W)}.$$

When minimizing models that involve $q_k(W)$, we consistently approximate the gradient using the STE and treat α as if it were independent of W .

D Comparizon of soft-orthogonal regularizers

In addition to the *soft-orthogonality* regularizer $R^{SO} = \|W W' - I\|_F^2$, we tested another regularizer that we term the *Spectral regularizer*: $R^{spectral}(W) = \sum_{i=1}^{n_h} |\sigma_i - 1|^2$, where $(\sigma_i)_{i=1}^{n_h}$ represents the singular values of W . The computation of this regularizer and its gradient involves performing the singular value decomposition of W , which becomes computationally expensive for large hidden size values n_h .

We present the results of STE-pen with this regularizer on pMNIST and compare these results with those of the SO regularizer. In Figure 6, we display the accuracies and ratios $\sigma_{\min}(q_k(W))/\sigma_{\max}(q_k(W))$ for various hidden sizes n_h . Although the results for both regularizers are similar, the SO regularizer is computationally more efficient.

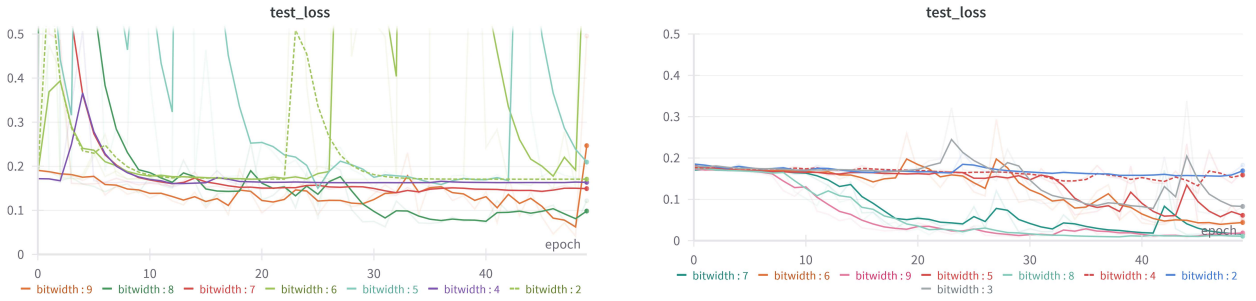


Figure 7: Evolution of Test Loss During Training for the Adding task with $n_h = 170$. (Left) STE-projUNN ; (Right) STE-Bjorck.

E Complements on the Adding task experiments

Detailed task description: The *Adding task* as described in [Arjovsky et al., 2016] defines as input two parallel data sequences of length T , concatenated in a time series in $(\mathbb{R}^2)^T$. The first sequence consists of scalars sampled independently and uniformly from the interval $[0, 1]$. The second sequence consists of zeros, except for two entries that are set to 1. The positions of the first and second occurrences of 1 are randomly selected, each following a uniform distribution over the intervals $\llbracket 1, T/2 \rrbracket$ and $\llbracket T/2 + 1, T \rrbracket$, respectively. The output is the sum of the two scalars from the first sequence, located at the positions corresponding to the 1s in the second sequence. As T increases, this task transforms into a problem requiring longer-term memory. Naively predicting 1 (the average value of the sum of two independent random variables uniformly distributed in $[0, 1]$) for any input sequence yields an expected mean squared error (MSE) of ≈ 0.167 , serving as our naive baseline.

Hyperparameters: We use as in [Kiani et al., 2022], 100000 training samples, and 2000 test samples.

As described in [Kiani et al., 2022], initialization is done with the identity matrix. For all approaches, we use *ReLU* as the activation function σ .

We do not detail hyperparameters for the STE-pen method here, as none of the tested configurations yields satisfactory results.

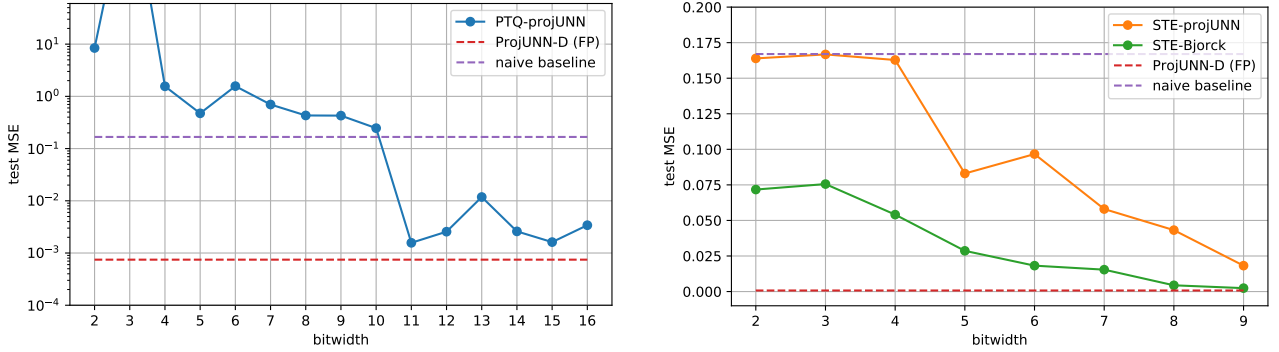
The initial learning rate is $1e-4$ for projUNN-D (i.e. projUNN (FP), PTQ-projUNN and STE-projUNN strategies), and $1e-3$ for STE-Bjorck. A divider factor of 32 is applied for recurrent weights update, as described in [Kiani et al., 2022]. A learning rate schedule is applied by multiplying the learning rate by 0.94 at each epoch. We use RMSprop optimizer for projUNN-D (i.e. projUNN (FP), PTQ-projUNN and STE-projUNN strategies) method, applying the projUNN-D algorithm with the LSI sampler and a rank 1 (as described in [Kiani et al., 2022]). For STE-Bjorck we use the classical Adam optimizer. Batch size is set to 50.

The training spanned 50 epochs.

For LSTM (FP), our results align with those reported in [Helfrich et al., 2018], demonstrating its capability to learn this task even over 750 time steps.

Complementary results: We present on Figure 7 the evolution of test loss during the training for STE-projUNN and STE-Bjorck and several bitwidths. The curves verify that STE-Bjorck learns the adding-task with greater ease.

We present on Figure 8 the test accuracy for a larger hidden size $n_h = 400$, for PTQ-projUNN, STE-projUNN, STE-Bjorck, and projUNN (FP). Conclusions are similar to the ones established for $n_h = 170$ for PTQ-projUNN, STE-projUNN and STE-Bjorck. When compared to the results displayed on Figure 2, the results of STE-projUNN and STE-Bjorck improve. In particular, STE-Bjorck significantly beats the naive baseline even for $k = 2$.

Figure 8: Adding task results for $T = 750$ and $n_h = 400$.

F Complements on the Copy task experiments

Detailed task description: This task is the same experiment as in [Wisdom et al., 2016], based on the setup defined by [Hochreiter and Schmidhuber, 1997, Arjovsky et al., 2016]. The copy task is known to be a difficult long-term memory benchmark, that classical LSTMs struggle to solve [Arjovsky et al., 2016, Helfrich et al., 2018].

Here, input data examples are in the form of a sequence of length $T = T_0 + 20$, whose first 10 elements represent a sequence for the network to memorize and copy. We use a vocabulary $V = \{a_i\}_{i=1}^p$ of $p = 8$ elements, plus a blank symbol a_0 and a delimiter symbol a_{p+1} . Each symbol a_i is one-hot encoded, resulting in an input time series where $n_i = 10$ and an output time series where $n_o = 9$ (a_{p+1} is not a target value).

An input sequence has its first 10 elements sampled independently and uniformly from V , followed by T_0 occurrences of the element a_0 . Then, a_{p+1} is placed at position $T_0 + 11$, followed by another 9 occurrences of a_0 . The RNN is tasked with producing a sequence of the same length, $T_0 + 20$, where the first $T_0 + 10$ elements are set to a_0 , and the last ten elements are a copy of the initial 10 elements of the input sequence.

The naive baseline consists of predicting $T_0 + 10$ occurrences of a_0 followed by 10 elements randomly selected from V . Such a strategy results in an expected cross-entropy of $\frac{10 \log 8}{T_0 + 20}$.

Hyperparameters: We use as in [Kiani et al., 2022], 512000 training samples, and 100 test samples.

As described in [Kiani et al., 2022], for projUNN-D (i.e. projUNN (FP), PTQ-projUNN and STE-projUNN strategies), we use Henaff initialization [Henaff et al., 2016]. For all approaches, we use *modReLU* as the activation function σ [Helfrich et al., 2018].

As for the Adding task, we do not detail hyperparameters for the STE-pen method here.

The initial learning rate is $7e-4$ for projUNN-D (i.e. projUNN (FP), PTQ-projUNN and STE-projUNN strategies), and $1e-4$ for STE-Bjorck. A divider factor of 32 is applied for recurrent weights update, as described in [Kiani et al., 2022]. A learning rate schedule is applied by multiplying the learning rate by 0.9 at each epoch. We use the RMSprop optimizer for projUNN-D (i.e. projUNN (FP), PTQ-projUNN and STE-projUNN strategies), applying the projUNN-D algorithm with the LSI sampler and a rank 1 (as described in [Kiani et al., 2022]). For STE-Bjorck we use the classical Adam optimizer. Batch size is set to 128.

The training spanned 10 epochs.

For LSTM (FP) we report the results given by [Wisdom et al., 2016], which indicates that it remains stuck at the naive baseline.

Complementary results: We present on Figure 9 the evolution of test loss during the training for STE-projuNN and STE-Bjorck and several bitwidths.

We present the results for the copy task in Figure 10 with $T_0 = 1000$ time steps and $n_h = 190$. The conclusions drawn are similar to those depicted in Figure 3, where $T_0 = 1000$ and $n_h = 256$. The main difference between the results in Figure Figure 10 for $n_h = 190$ and Figure 3 for $n_h = 256$ lies in the fact that, similar to the adding task, a smaller value

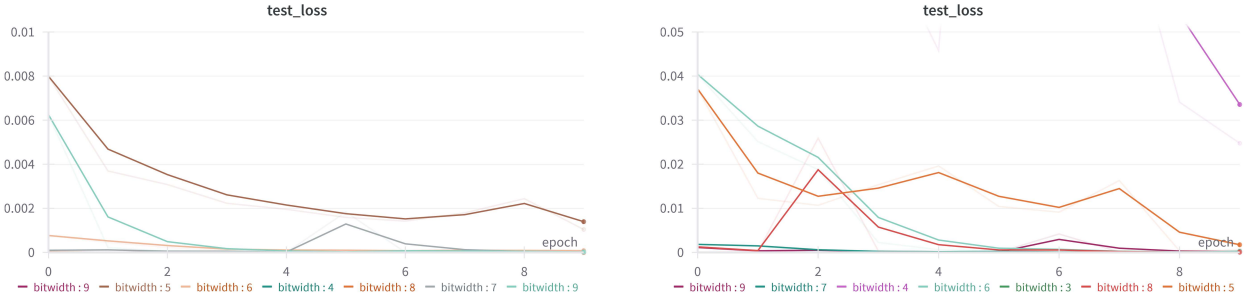


Figure 9: Evolution of Test Loss During Training for the Copy task with $n_h = 256$. (Left) STE-projUNN ; (Right) STE-Bjorck.

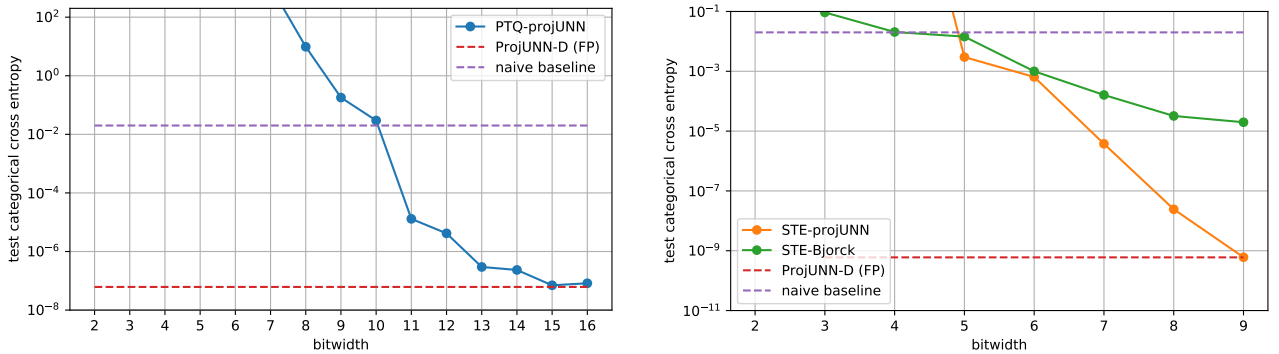


Figure 10: Copy task results for $T = 1000 + 20$ and $n_h = 190$.

of n_h allows achieving comparable performance but with a larger bitwidth k . There appears to be a trade-off that needs to be optimized between hidden size and bitwidth.

We present the results for the copy task in Figure 11 with $T_0 = 2000$ time steps and $n_h = 256$. This task proves to be more challenging to learn; both STE-projUNN and STE-Bjorck only achieve the naive baseline with 6-bit quantization. It seems likely that increasing the hidden size n_h would allow for a reduction in bitwidth.

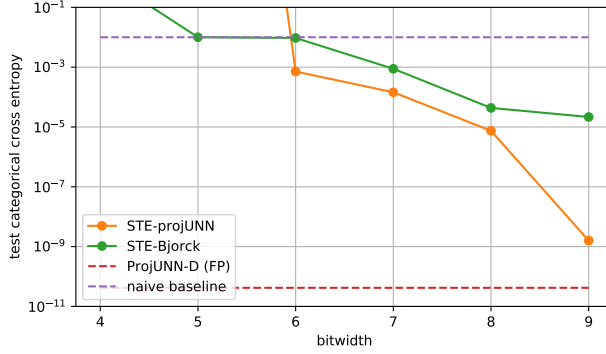
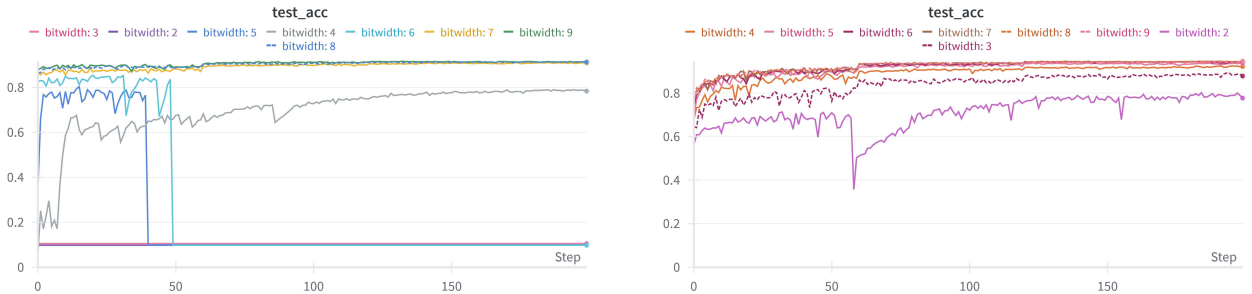
G Complements on the pMNIST task experiments

Hyperparameters: We use the 60,000 training samples and 10,000 test samples from the MNIST dataset.

As described in [Kiani et al., 2022], we employ a random orthogonal matrix initialization for the recurrent weight matrix. The activation function σ is *ReLU* for STE-Bjorck and STE-pen and LSTM (FP). We utilize *modReLU* [Helfrich et al., 2018] for projUNN-D (i.e. projUNN (FP), PTQ-projUNN and STE-projUNN strategies), as performances achieved with ReLU are inferior.

The initial learning rate is $1e - 3$ for all strategies and weights. It remains constant for STE-pen and LSTM (FP). A learning rate schedule is applied by multiplying the learning rate by 0.2 every 60 epochs for projUNN-D (i.e. projUNN (FP), PTQ-projUNN and STE-projUNN strategies) and STE-Bjorck.

We utilize the RMSprop optimizer for projUNN-D (i.e. projUNN (FP), PTQ-projUNN and STE-projUNN strategies), implementing the projUNN-D algorithm with the LSI sampler and a rank of 1 (as described in [Kiani et al., 2022]). For STE-Bjorck, STE-pen and LSTM (FP), we employ the classical Adam optimizer.

Figure 11: Copy task results for $T = 2000 + 20$ timestep with $n_h = 256$.Figure 12: Evolution of the Accuracy During Training for pMNIST with $n_h = 170$. (Left) STE-projUNN ; (Right) STE-Bjorck.

For STE-pen, the regularization parameter λ , which governs the trade-off between optimizing the learning objective and the regularizer (see Equation (5)), is set to $1e - 1$.

The batch size is set to 64 for STE-pen and LSTM (FP). For all other approaches, it is set to 128.

The training spanned 200 epochs.

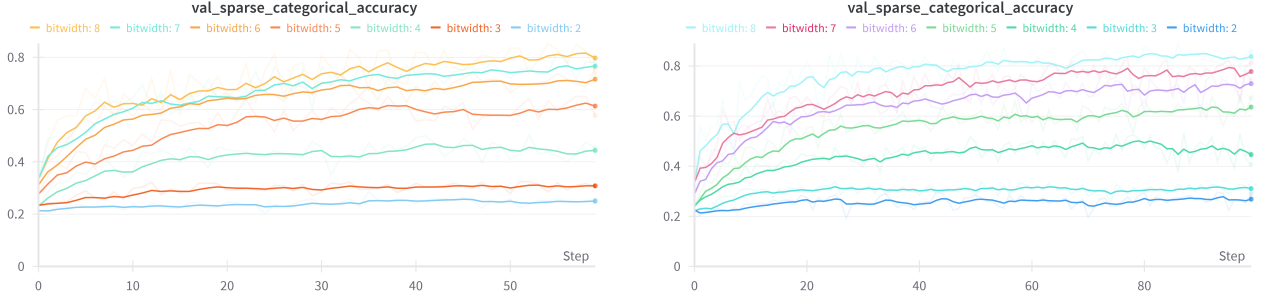
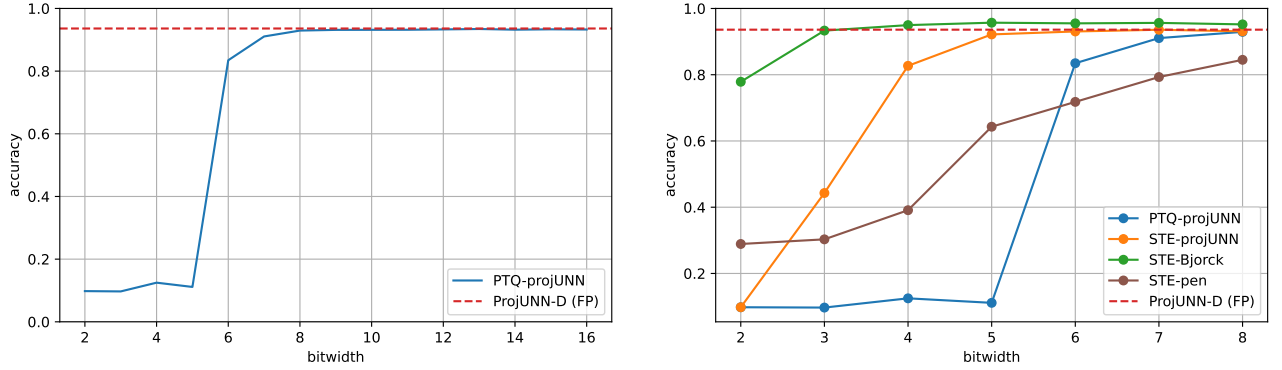
Complementary results: We present on Figure 12 the evolution of test accuracy during the training for STE-projUNN and STE-Bjorck and several bitwidths. Learning is easier with STE-Bjorck.

On Figure 13, we illustrate the accuracy evolution during training for STE-pen and various bitwidths with $n_h = 170$ and $n_h = 360$.

We present the results for pMNIST in Figure 14 with a larger hidden size, $n_h = 360$. The qualitative conclusions drawn are similar to those depicted in Figure 4 for $n_h = 170$. Similar to the Adding task and the copy task, the results for the larger hidden size are superior. For instance, PTQ-projUNN achieves an accuracy above 80% for bitwidth $k = 6$, while the case of $n_h = 170$ required 8 bits to reach comparable results (see Figure 4-a).

H Complements on the Character level Penn TreeBank experiments

Detailed task description: The Penn TreeBank dataset consists of sequences of characters, utilizing an alphabet of 50 different characters. The dataset is divided into 5017K training characters, 393K validation characters, and 442K test characters. Sentences are padded with a blank value when their size is less than the fixed sequence length of 150 characters. The task aims to predict the next character based on the preceding ones. Formally expressed as time series,

Figure 13: Evolution of the Accuracy During Training for pMNIST with STE-pen (Left) $n_h = 170$ (Right) $n_h = 360$.Figure 14: pMNIST results for $n_h = 360$

each sentence represents an input time series of size $n_i = 50$ (since characters are one-hot encoded) with $T = 150$, and the corresponding output time series is identical to the input time series but shifted by one character.

The models are evaluated using the Bit Per Character measure (BPC), which is the base-2 logarithm of the likelihood on masked outputs (to exclude padding values for evaluation).

Hyperparameters: As described in [Kiani et al., 2022], we take a random orthogonal matrix initialization for the recurrent weights. We use *ReLU* as the activation function σ for STE-Bjorck and STE-pen. For projUNN-D (i.e., projUNN (FP), PTQ-projUNN and STE-projUNN strategies), we utilize *modReLU* [Helfrich et al., 2018] as the activation function, as performances achieved with ReLU were found to be inferior.

The initial learning rate is set to $1e - 3$ for all strategies and weight types. It remains constant for STE-pen and LSTM (FP). A divider factor of 8 is applied to recurrent weight updates. A learning rate schedule is implemented by multiplying the learning rate by 0.2 every 20 epochs for projUNN-D (i.e., projUNN (FP), PTQ-projUNN, and STE-projUNN strategies) as well as for STE-Bjorck.

We employ the RMSprop optimizer for projUNN-D, utilizing the projUNN-D algorithm with the LSI sampler and a rank 1, as described in [Kiani et al., 2022]. For STE-Bjorck, STE-pen, and LSTM (FP), we use the classical Adam optimizer.

The regularization parameter λ for STE-pen is fixed to $1e - 1$.

The batch size is set to 100 for STE-pen and LSTM (FP). For all other approaches, it is set to 128.

The training spanned 50 epochs.

Complementary results: We present on Figure 15 the evolution of validation BPC during training for STE-pen and several bitwidths with $n_h = 1024$ and $n_h = 2048$.

Figure 16 presents supplementary results for a larger hidden size of $n_h = 2048$. While most results are similar to those obtained with $n_h = 1024$, it is worth noting that STE-projUNN trainings did not converge for bitwidths 4 and 7.

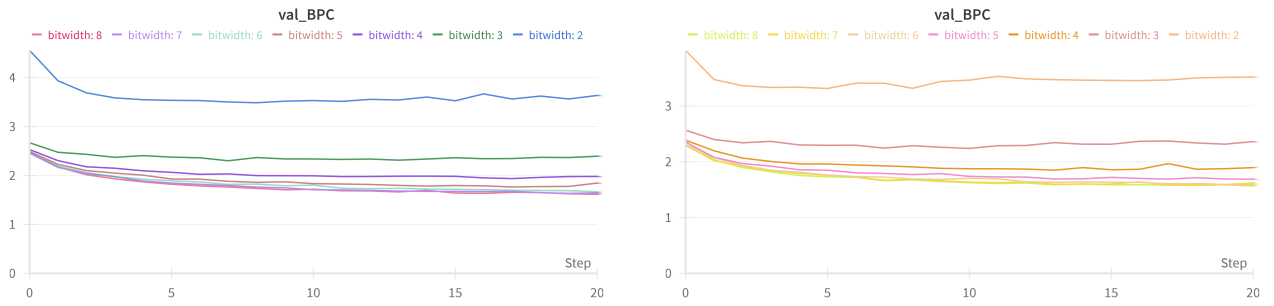


Figure 15: Evolution of the BPC During Training for Penn TreeBank with STE-pen (Left) $n_h = 1024$ (Right) $n_h = 2048$.

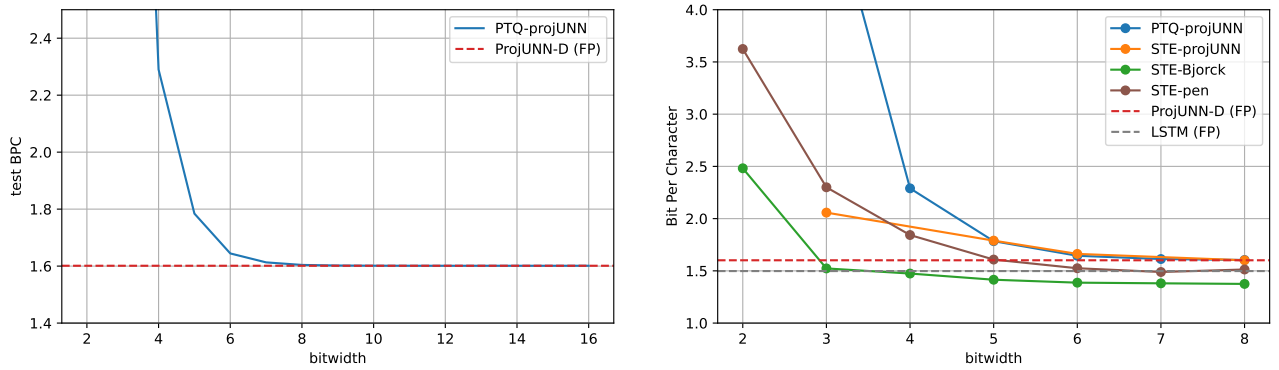


Figure 16: Penn TreeBank results for $n_h = 2048$. The STE-projUNN curve has no dots at $k = 2, k = 4, k = 7$, indicating that the training diverged.